

Evolution of the Climate as an Attributable Complex System with Main Cause

Liaofu Luo ^{1,*} and Jun Lv ^{2,*}

¹ Faculty of Physical Science and Technology, Inner Mongolia University, 235 West College Road, Hohhot 010021, China; lolfcm@imu.edu.cn

² College of Science, Inner Mongolia University of Technology, 49 Aymin Street, Hohhot 010051, China; lujun@imut.edu.cn

* Correspondence: lolfcm@imu.edu.cn (L.L.); lujun@imut.edu.cn (J.L.); Tel.: +86-471-4992676 (L.L.); +86-13039500654 (J.L.)

Peer review status:

The paper is a non-peer reviewed preprint submitted to EarthArXiv.

Abstract

Attributable complex systems can be classified into two categories: those with a main cause and those without. The climate is an attributable complex system with a main cause, where CO₂ concentration serves as the primary fingerprint. The essential dynamics of climate change can be effectively captured through the representation of CO₂ concentration. In this study, we analyze global warming in detail, discovering that historical CO₂ concentration data can be well described by exponential growth. Extending the simulation of CO₂ concentration changes from 2015 to 2500 within the framework of Shared Socioeconomic Pathways (SSPs), we observe a transition from exponential growth to exponential decay in the later stages. To model this shift, we introduce a modified exponential function. Additionally, by accounting for natural climate variability and examining the correlation between global temperature anomalies and CO₂ concentrations, we find that this correlation becomes evident only over the long term. Using this relationship and CO₂ concentration data, we generate predictions for global temperature anomalies up to 2500, which can be compared with other models in the literature.

Keywords: attributable complex system, global warming, carbon dioxide concentration, data-driven prediction

Introduction

Global warming represents a significant challenge to Earth's ecosystem [1,2]. Extensive studies on climate change, through observational detection and attribution, consistently underscore its anthropogenic origins [3-6]. The Intergovernmental Panel on Climate Change (IPCC) has synthesized observational data, concluding that human emissions—particularly CO₂ since the Industrial Revolution—are the primary drivers of climate change. This consensus has spurred global efforts by scientists and policymakers to develop strategies for mitigating climate change.

The climate system is a quintessential example of a complex system, evolving over time. Detecting, attributing, and predicting climate change from the perspective of complex system theory is a key issue of public concern. As we know, complex system theory has advanced significantly in recent years. Whitney first proposed that high-dimensional systems often contain redundant information and that their essential dynamics can be captured through low-dimensional representations [7]. In the context of detecting strange attractors in turbulence, Takens introduced a theorem on delay embedding, suggesting that each time series variable in a dynamical system can be used to reconstruct a low-dimensional representation, allowing for an isomorphic reconstruction of the original system from a single time series [8]. As a result, low-dimensional representations can serve as generalized predictors, enabling the identification of future dynamics in complex systems. Recently, Wutao et al. generalized the concept of low-dimensional embedding for complex systems by combining feature embedding with delay embedding, demonstrating the potential of this new approach for applications in real-world systems [9]. Lucarini and Chekroun showed that response theory for nonequilibrium systems

provides the physical and dynamical foundation for the optimal fingerprinting method (OFM), and they extended the OFM to the nonlinear response regime [10].

The detection, attribution, and prediction of climate change through the lens of complex system theory is an area of intense interest. Beginning with the study of attributable complex systems, we classify complex systems into two categories, demonstrating the existence of a specific category, termed the Attributable Complex System with Main Cause (ACSMC). We argue that the climate system falls under the ACSMC category, with CO₂ emissions as the primary driver and CO₂ concentration as the forcing pattern. With this understanding, we can approach global climate warming from a data-driven perspective.

Historical simulations play a crucial role in understanding future climate dynamics. The IPCC introduced several Shared Socio-economic Pathways (SSPs) to project future greenhouse gas concentrations from 2015 onwards, spanning nine scenarios. Notably, SSP1-1.9 aligns closely with the Paris Agreement's 1.5°C target, while other scenarios, such as SSP1-2.6, SSP2-4.5, SSP3-7.0, and SSP5-8.5, are frequently emphasized in the research community (see IPCC Sixth Assessment Report [2]).

Traditionally, climate change research has focused on understanding how greenhouse gases impact the atmospheric energy balance and the physical mechanisms of the global carbon cycle. Due to the inherent complexity of the system, accounting for every detail remains a challenge. However, by recognizing the system as an Attributable Complex System with Main Cause, we propose an alternative, data-driven approach. By analyzing historical CO₂ concentration data, we will develop time-dependent parameter models and extend these models to future projections across the five SSP scenarios.

In applying response theory for nonequilibrium systems to study climate change, it is essential to account for natural climate variability. Global warming, defined as the long-term change in global average temperature from 1850 to 2020, does not follow a consistent annual increase. Using historical data, we establish a linear relationship between temperature anomalies and CO₂ concentrations over extended periods (seven years or more). By synthesizing these insights, we project global temperature changes up to the year 2500 under each SSP scenario and compare these projections with global surface air temperature (GSAT) forecasts (for the period before 2300) from other models in the IPCC Sixth Assessment Report (AR6) [2].

Data and Methods

Historical temperature anomaly data

The temperature anomaly data from 1880 to 2023 were obtained from NASA/GISS/GISTEMP [11]. This dataset provides the 12-month running mean of temperature anomalies with a base period of 1880 to 1930. The data source selected is the Global Historical Climatology Network version 4 (GHCN v4) and Extended Reconstructed Sea Surface Temperature version 5 (ERSST v5).

Historical data on CO₂ concentration variation

The monthly-average atmospheric CO₂ concentration data at Mauna Loa Observatory from 1958.3 to 2023.12 were obtained from the Scripps CO₂ Program [12].

Historical data on CO₂ emissions per year

The data on CO₂ emissions per year from 1850 to 2023 were obtained from the Global Carbon Project [13].

Data on future CO₂ concentrations under five SSP scenarios

The data on future CO₂ concentrations under five Shared Socioeconomic Pathways (SSP) scenarios from 2015 to 2500 were obtained from the Greenhouse Gas Concentrations dataset of The University of Melbourne [14].

Data on future warming under five SSP scenarios

The data on the change in global surface air temperature up to 2300 under five SSP scenarios were derived from Figure 4.40 in Chapter 4 of the Sixth Assessment Report (AR6) [15].

Methodology

In this study, we used the non-linear least squares method to analyze observational data on CO₂ concentration, emissions, temperature anomalies, and their interrelationships. For each case, we determined the model parameters and assessed the goodness of fit using the R-squared (R^2) value. A two-sided p -value of < 0.001 was considered as statistically significant; the p -value was calculated based on the F-statistic. Additionally, we reported the root mean squared error (RMSE) for each simulation.

Results

1, Classification of Attributable Complex System

Using the response theory for nonequilibrium systems, the observables Y_k ($k=1, \dots, S$) can be expressed as a linear combination of response patterns

$$Y_k = \sum_{p=1}^M x_k^p \quad (k=1, \dots, S), \quad (\text{A})$$

where x_k^p represents the M characteristics (or fingerprints), each associated with a distinct forcing factor. The generality of this equation can be understood as follows: the interaction between these characteristics should contribute second-order adjustments on the right-hand side of the equation. However, the additional M^2 fingerprints can be eliminated through linear regression [10]. Equation (A) serves as a foundation for classifying an attributable complex system. If the magnitude estimate

$$|Y_i| / \sum_k^S |Y_k| \cong O(1), \quad (\text{B})$$

(where $|Y_i|$ and $|Y_k|$ denote the magnitudes of Y_i and Y_k , respectively) holds for some i , then the system is classified as an Attributable Complex System with Main Cause (ACSMC). Conversely, if Equation (B) does not hold for any i , the system is categorized as an Attributable Complex System without Main Cause (ACSN-C).

Given the established understanding that human emissions—particularly CO₂ emissions—are the primary drivers of global warming [3-6], we conclude that Equation (B) is satisfied for the climate system, with CO₂

concentration serving as the main fingerprint.

We hypothesize that this classification framework for attributable complex systems will have wide applicability in various domains, including quantitative social sciences, in addition to climate science. The ACSMC satisfies Whitney's embedding theorem [7], meaning its evolution can be captured through a low-dimensional representation. On the other hand, for ACSN-C systems, predicting their evolution remains highly challenging due to the lack of a clear primary cause.

2, Simulation of historical data for CO₂ concentration and the data from 2015 to 2500 in five SSP scenarios

Simulation of historical data for CO₂ concentration The historical CO₂ concentration data (Fig. 1a) can be effectively modeled using exponential functions. The parameters of these exponential models are defined and derived.

Using the exponential function

$$C = A \cdot \exp[B(t - t_0)] + c_0, \quad (A = 55.408, B = 0.016581, c_0 = 258.61, t_0 = 1958), \quad (1)$$

we accurately simulated the annual variation in CO₂ concentration from 1958 to 2023 at the Mauna Loa Observatory (Fig. 1b).

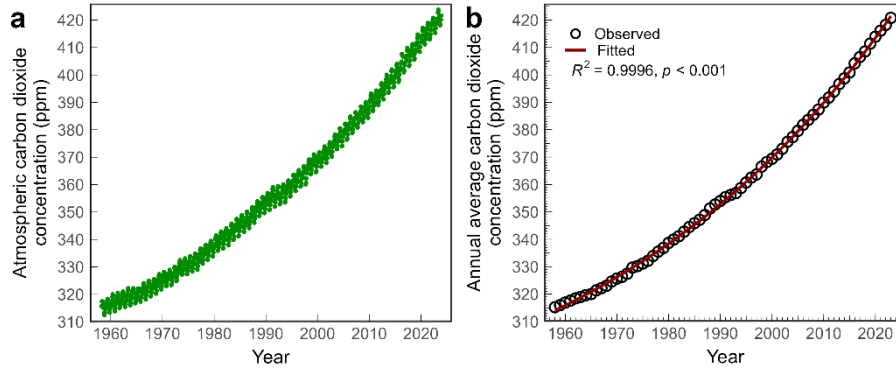


Fig. 1. Atmospheric CO₂ concentration from March 1958 to December 2023. (a) The Keeling Curve (The monthly-averaged data from the Mauna Loa Observatory [12]). (b) Simulation of the annual variation in CO₂ concentration.

Simulating CO₂ concentration from 2015 to 2500 in five SSP scenarios The time-dependent parameter representation of CO₂ concentration from 2015 to 2500 is derived using five Shared Socioeconomic Pathway (SSP) concentration projections. Two distinct exponential functions are formulated for the early and late stages within each SSP scenario.

Using the reduced-complexity climate-carbon-cycle model MAGICC7.0 [16], the historical CO₂ concentration data is extended from 2015 to 2500. To obtain the time-dependent parameter representation for each of the five scenarios, we generalize the exponential function based on the historical dataset and assume

$$C = a \cdot \exp[\alpha(t - y_0) - \beta(t - y_0)^\lambda], \quad t \in [y_0, y], \quad (2a)$$

$$C = C_y \cdot \exp[-\gamma(t - y)], \quad t \in [y, 2500], \quad (2b)$$

(where a and C_y are determined by continuity conditions of C at $t=y_0=2015$ and $t=y$), to simulate the concentration as described in the literature [14]. The results are shown in Fig. 2 and detailed in Table 1.

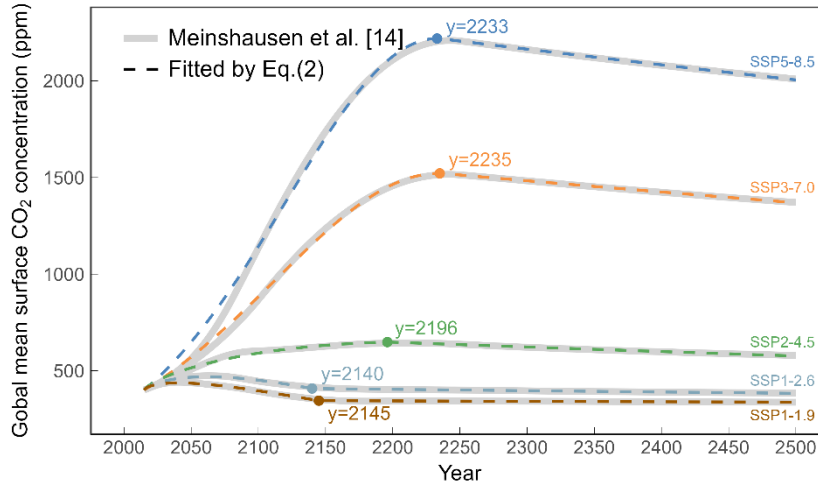


Fig. 2. Simulation of the CO₂ concentration from 2015 to 2500 in five SSP scenarios

Table 1 Best-fit parameters in simulation and related goodness R^2

Scenario	a	α	β	λ	$R^2(2a)$	y	$\gamma(\times 10^{-4})$	$R^2(2b)$
SSP5-8.5	399.95	0.01462	1.3102×10^{-5}	2.1601	0.9957	2233	3.8142	0.9979
SSP3-7.0	399.95	0.01054	2.8431×10^{-6}	2.3645	0.9973	2235	3.9860	0.9993
SSP2-4.5	399.95	-0.01048	-0.03365	0.8192	0.9741	2196	3.8818	0.9932
SSP1-2.6	399.95	-0.07201	-0.08954	0.9553	0.9487	2140	1.7408	0.9721
SSP1-1.9	399.95	-0.01015	-0.03086	0.7472	0.9903	2145	0.6379	0.8522*

* Note: $R^2(2b)$ for SSP1-1.9 lower than others may be due to the small value of γ . The lack of uncertainty estimates in Meinshausen's concentration projection [14] should also be noticed.

By synthesizing simulations of both historical and projected CO₂ concentration data from 2015 to 2500, we find that CO₂ concentration follows two distinct time-dependent patterns. Before 2015 and after time y (with y varying between 2140 and 2235 across the five SSP scenarios), the concentration follows a pure exponential growth (with $\lambda=1$). Between 2015 and y , the concentration follows a modified exponential function (with $\lambda \neq 1$). Prior to 2015, the pure exponential model shows an increasing trend, while after y , it exhibits a decreasing trend. The transition between these phases is governed by the modified exponential function, reflecting the influence of socio-economic pathways and political conditions. Above analyses show that CO₂ concentration can serve as an effective time series variable for reconstructing a low-dimensional representation of the complex climate system.

3 , Prediction on temperature anomaly from CO₂ concentration data

The linear relationship between temperature anomaly and CO₂ concentration in the long term The correlation between temperature anomalies and CO₂ concentration is thoroughly examined, revealing a linear relationship over extended periods. Temperature anomaly data from 1880 to 2023 are based on a 12-month moving average, while monthly CO₂ concentration data from 1958 to 2023 are sourced from measurements at the Mauna Loa Observatory. Direct comparisons between immediate temperature anomalies and CO₂ concentration values are not meaningful, as the physical correlation between climate change and CO₂ emissions becomes evident only over the long term. After extensive statistical analysis, it is determined that "long term" refers to periods of data

averaging longer than seven years. All simulations should therefore follow this consistent long-term timeframe.

The following diagrams illustrate the relationship between temperature anomaly and CO₂ concentration from 1958 to 2022, using one-year, seven-year, thirteen-year, and seventeen-year moving averages (with a one-month step) (see Fig. 3). Notably, a high goodness of fit (R^2 -squared value of 0.99) is achieved when using seven-year or longer averaging periods. Thus, the linear correlation between temperature anomaly and CO₂ concentration is best established over periods of seven years or more. The outcome of strong linear regression is easily understood, as natural temperature fluctuations follow irregular 2-7 year cycles. Consequently, natural climate variability can be accounted for in this study by employing a moving average method with a window of seven years or more.

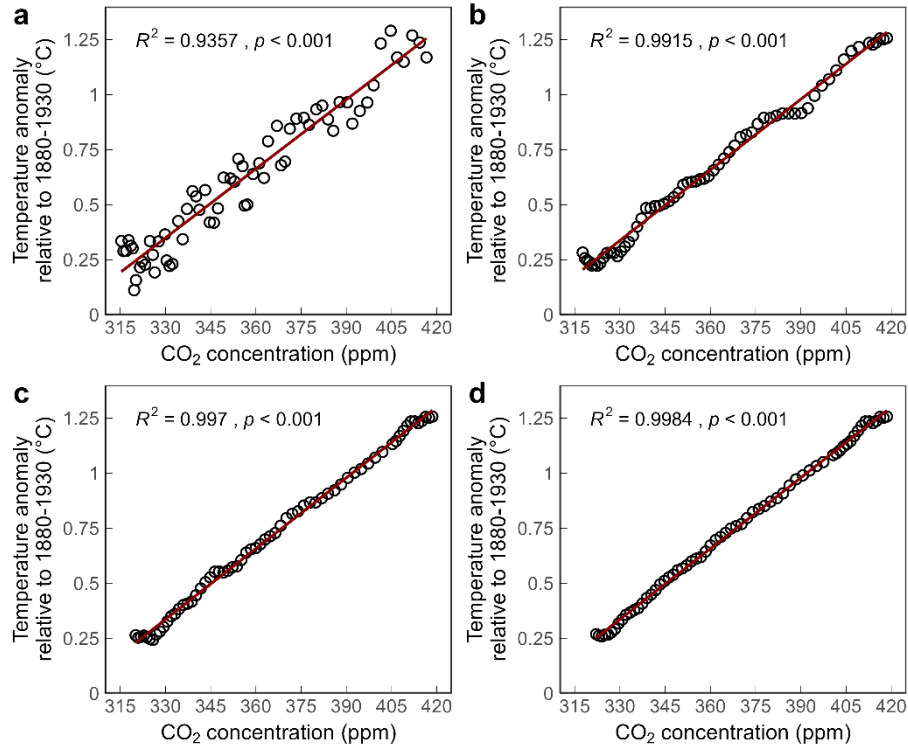


Fig. 3. Relationship between temperature anomaly and CO₂ concentration. (a) one-year, (b) seven-years, (c) thirteen-years, and (d) seventeen-years running mean (with step one month). Temperature anomaly data are taken from [11] and CO₂ concentration data are taken from [12]. The solid line represents the linear regression.

Predicting global temperature anomaly To forecast global temperature anomaly $T(\text{Pred})$, we use its linear relationship with CO₂ concentration C , expressed as $T(\text{Pred})=kC+b$. First, we validate this relationship using historical data before applying it to assess both near-term and long-term scenarios.

Substituting Eq. (1) into the linear relationship between $T(\text{pred})$ and CO₂ concentration, we obtain

$$T(\text{Pred}) = k_1\{A \cdot \exp[B(t - t_0)] + c_0\} + b_1, \quad t \in [1958,2023]. \quad (3)$$

This equation is interpreted in the context of a seven-year or longer moving average, as discussed earlier. The optimal values for k_1 and b_1 are provided in Table 2.

For both near-term (2015 to y) and long-term (from y to 2500) projections, we propose the following models

$$T(\text{Pred}) = k_2\{a \cdot \exp[\alpha(t - y_0) - \beta(t - y_0)^\lambda]\} + b_2, \quad t \in [2015, y], \quad (4a)$$

$$T(\text{Pred}) = k_2 \{ C_y \cdot \exp[-\gamma(t - y)] \} + b_2, \quad t \in [y, 2500], \quad (4b)$$

where the parameters α , β , λ , and γ are provided in Table 1. The optimal values for k_2 and b_2 , derived from simulations of Eqs. (4a) and (4b), are detailed in Table 2. Comparisons between $T(\text{pred})$ and projected temperature anomalies from existing literature [15] are shown in Fig. 4.

Table 2 Parameters in relation of temperature anomaly with CO₂ concentration

Scenario	k_1 (°C/ppm)*	b_1 (°C)*	k_2 (°C/ppm)	b_2 (°C)
SSP5-8.5			0.0044	-0.61
SSP3-7.0	0.01070	-3.192	0.0061	-1.29
SSP2-4.5	(0.01072)	(-3.202)	0.0087	-2.33
SSP1-2.6			0.0099	-2.81
SSP1-1.9			0.0075	-1.85

*All parameters are obtained in 7-year average except the values of k_1 and b_1 inside the parentheses in 2nd and 3rd columns of the table which is obtained in 17-year average for comparison. We found there is litter difference between these two averages.

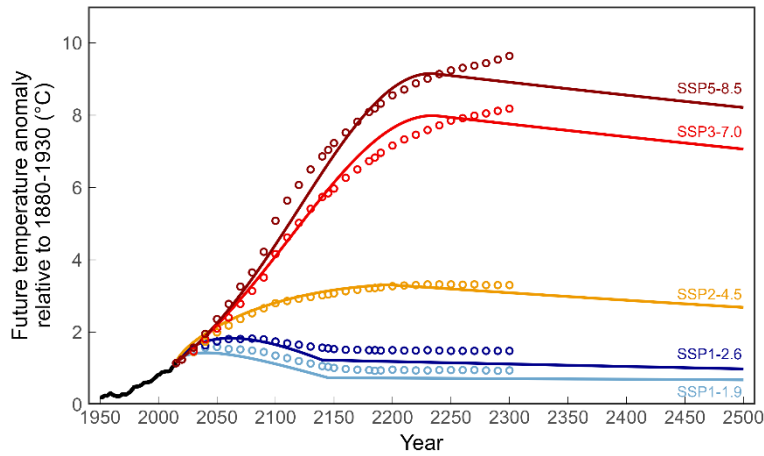


Fig. 4. Changes of predicted temperature anomaly $T(\text{Pred})$ from 2015 to 2500 in five SSP scenarios. The solid lines, each represented by a different color, correspond to $T(\text{Pred})$ (2015 to 2500) calculated from Eqs. (4a) and (4b) in the five SSP scenarios. Additionally, the projections of temperature anomalies up to 2300, sourced from Figure 4.40 in Chapter 4 of AR6, are represented by small cycles [15]

Note that the above results of prediction on temperature anomaly in Fig. 4 can be largely improved when the 99% confidence intervals of CO₂ concentration for each SSP scenario are considered and the continuity of the path of concentration variation at time y is taken into account (see <https://doi.org/10.21203/rs.3.rs-4495753/v2>).

We have shown that the predicted temperature anomalies $T(\text{Pred})$ from 2015 to 2300 are basically consistent with projections in the literature if the inherent uncertainty in the temperature anomaly projections is considered (see Table 4.9 in [15]). Additionally, the present approach extends the GSAT forecast up to 2500. This predictive framework provides valuable insights into the trajectory of global temperature anomalies, supporting proactive measures to mitigate climate change impacts.

To summarize, our analysis shows that carbon dioxide concentration serves as an effective indicator for the evolution of the climate system. Since high-dimensional systems often contain redundant information, with their key characteristics potentially represented in lower-dimensional forms [7], our data-driven predictions of global temperature anomalies indicate that low-dimensional embedding is a powerful approach for studying the climate system. This method aligns with techniques commonly used in the analysis of other complex systems

[8-10].

Acknowledgements

We express our gratitude to Dr Ying Zhang for her assistance with data collection, valuable discussions, and insightful suggestions.

Author contributions

L.-L.: conceptualization, methodology, investigation, writing—original draft; J.-L.: methodology, investigation, data curation, writing- review and editing, visualization.

Competing interests

The authors declare no competing interests.

Data availability

Historical temperature anomaly data for GISTEMP is available at https://data.giss.nasa.gov/gistemp/zonal_means, and for HadCRUT5 at <https://climate.metoffice.cloud/temperature.html#datasets>. Historical CO₂ concentration data can be accessed at https://scrippsco2.ucsd.edu/data/atmospheric_co2/primary_mlo_co2_record.html. Historical CO₂ emissions data is available at <https://www.icos-cp.eu/science-and-impact/global-carbon-budget/2024>. Data on future CO₂ concentrations under five Shared Socioeconomic Pathways (SSPs) scenarios can be found at <https://greenhousegases.science.unimelb.edu.au/#!/view>. Data on changes in global surface air temperature up to 2300 under these five SSP scenarios is available at <https://gitlab.com/magicc/ar6-wg1-plots-and-processing>.

References

1. McCulloch, M.T., Winter, A., Sherman, C.E. & Trotter, J. A. 300 years of sclerosponge thermometry shows global warming has exceeded 1.5 °C. *Nat. Clim. Chang.* **14**, 171-177 (2024).
2. IPCC. Summary for policymakers in *Climate change 2021-The physical science basis* (eds Masson-Delmotte, V. et al.) 3-32 (Cambridge University Press, 2023).
3. Manabe, S. & Wetherald, R. T. Thermal equilibrium of the atmosphere with a given distribution of relative humidity. *J. Atmos. Sci.* **24**, 241-259 (1967).
4. Hasselmann, K. On the signal-to-noise problem in atmospheric response studies, in *Meteorology of tropical oceans* (ed. Shaw, D. B.) 251-259 (R. Meteorol. Soc. 1979).
5. Manabe, S & Broccoli, A. J. *Beyond global warming: How numerical models revealed the secrets of climate change* (Princeton University Press 2019).
6. Hegerl, G. & Zwiers, F. Use of models in detection and attribution of climate change. *WIREs Climate Change* **2**, 570-591 (2011).
7. Whitney, H. Differentiable manifolds. *Ann. Math.* **37**, 645-680 (1936).
8. Takens, F. Detecting strange attractors in turbulence, in *Lecture notes in mathematics* (eds. Rand D. & Young L. S.) **898**, 366-381 (Springer Berlin Heidelberg, 1981).
9. Wu, T. et al. Predicting multiple observations in complex systems through low-dimensional embeddings. *Nat. Commun.* **15**, 2242 (2024).
10. Lucarini, V. & Chekroun, M. D. Detecting and attributing change in climate and complex systems: foundations, Green's

functions, and nonlinear fingerprints. *Phys. Rev. Lett.* **133**, 244201 (2024)

11. Lenssen, N. J. L. et al. Improvements in the GISTEMP uncertainty model. *JGR Atmospheres* **124**, 6307-6326 (2019).
12. Keeling, C. D. et al. Exchanges of atmospheric CO₂ and ¹³CO₂ with the terrestrial biosphere and oceans from 1978 to 2000. I. Global Aspects. *SIO Reference Series No. 01-06*, Retrieved from <https://escholarship.org/uc/item/09v319r9> (2001).
13. Friedlingstein, P. et al. Global carbon budget 2024. Preprint at <https://doi.org/10.5194/essd-2024-519> (2024).
14. Meinshausen, M. et al. The shared socio-economic pathway (SSP) greenhouse gas concentrations and their extensions to 2500. *Geosci. Model Dev.* **13**, 3571-3605 (2020).
15. Lee, J. Y. et al. Future global climate: scenario-based projections and near-term information in *Climate change 2021-The physical science basis* (eds Masson-Delmotte, V. et al.) 553-672 (Cambridge University Press, 2023).
16. Meinshausen, M., Raper, S. C. B. & Wigley, T. M. L. Emulating coupled atmosphere-ocean and carbon cycle models with a simpler model, MAGICC6 – Part 1: Model description and calibration. *Atmos. Chem. Phys.* **11**, 1417-1456 (2011).
17. Joint Committee for Guides in Metrology (JCGM). *Evaluation of measurement data - Guide to the expression of uncertainty in measurement (GUM 1995 with minor corrections)*. (2008).